The vibration properties of the (n,0) boron nitride nanotubes from ab initio quantum chemical simulations

The Vibration Properties of the (n,0) Boron Nitride Nanotubes from *Ab initio* Quantum Chemical Simulations.

A. Erba,[1] M. Ferrabone,[1] R. Orlando,[1] R. Dovesi,[1] and M. Rérat[2]

[1] *Dipartimento di Chimica and Centre of Excellence NIS (Nanostructured Interfaces and Surfaces), Università di Torino, via Giuria 5, IT-10125 Torino (Italy)*

[2] *Equipe de Chimie Physique, IPREM UMR5254, Université de Pau et des Pays de l'Adour, FR-64000 Pau (France)*

(Dated: August 23, 2012)

The vibration spectrum of single-walled zigzag Boron Nitride (BN) nanotubes is simulated with an *ab initio* periodic quantum chemical method. The trend towards the hexagonal monolayer (h-BN) in the limit of large tube radius R is explored for a variety of properties related to the vibrational spectrum: vibration frequencies, infrared intensities, oscillator strengths and vibration contributions to the polarizability tensor. The (n,0) family is investigated in the range from $n = 6$ (24 atoms in the unit cell and tube radius $R = 2.5$ Å) to $n = 60$ (240 atoms in the cell and $R = 24.0$ Å). Simulations are performed using the CRYSTAL program which fully exploits the rich symmetry of this class of one-dimensional periodic systems: $4n$ symmetry operators for the general (n,0) tube. Three sets of infrared active phonon bands are found in the spectrum. The first one lies in the 0 - 600 cm^{-1} range and goes regularly to zero when R increases; the connection between these normal modes and the elastic and piezoelectric constants of h-BN is discussed. The second (600 - 800 cm^{-1}) and third (1300 - 1600 cm^{-1}) sets tend regularly, but with quite different speed, to the optical modes of the h-BN layer. The vibrational contribution of these modes to the two components (parallel and perpendicular) of the polarizability tensor is also discussed.

I. INTRODUCTION

Carbon nanotubes are a class of materials with quasi one-dimensional (1D) structure which attract the attention of the scientific community due to their unique electrical, mechanical and thermal properties.[1,2] Given the structural analogy between graphite and hexagonal Boron Nitride (h-BN) monolayers, the existence of BN nanotubes was first proposed theoretically in 1994[3,4] and then proved experimentally soon after.[5] Even if graphite and h-BN exhibit the same structure and are isoelectronic, the corresponding nanotubes show many differences in their properties. In particular, BN nanotubes show a larger thermal stability and, thanks to a wide band gap ($\sim$ 5.5 eV), a less dramatic dependence of the electrical properties on rolling direction and tube diameter.[4] Such stability of the properties with respect to tube size is a major advantage of BN over Carbon nanotubes for which the poor control of tube size and chirality guaranteed by current synthesis techniques may result in a poor tuning of tube properties. As in the case of Carbon nanotubes, BN nanotubes are object of intense experimental[6–8] and theoretical[9–12] analysis, because of their possible applications as super-tough composite materials and components of nanoelectronic devices.

From a geometrical viewpoint, a single-walled BN nanotube may be regarded as the result of the rolling of a h-BN monolayer into a cylinder along a (n,m) lattice vector. The two integer indices n and m determine the diameter and chirality of the tube, that are the key parameters of their structure.[13,14]

The computational cost of quantum chemical simulations of these one-dimensional periodic systems, especially when performed at *ab inito* level, is rather high,[15–17] as nanotubes can contain dozens or hundreds of atoms in the unit cell, depending on rolling direction and tube radius. The rich symmetry which characterizes this class of materials, if adequately exploited, can drastically reduce their computational costs; interestingly, the symmetry of nanotubes increases with their size: for instance, the (n,0) family of Carbon and BN nanotubes exhibits $8n$ and $4n$ symmetry operators, respectively. When n increases along the series, the total number of atoms per cell increases linearly while the number of symmetry-irreducible atoms per cell remains constant: 2 for BN nanotubes. If these symmetry features are exploited, a *constant* scaling of the computational cost can be achieved with respect to the size of the system; the resulting reduction in computing time is dramatic.[18,19] A program, CRYSTAL,[20,21] which fully exploits both translational and point symmetry of the nanotubes is used for all calculations to be reported in this work. The additional exploitation of point symmetry permits to investigate tubes as huge as (100,0), about twice as huge as in our previous studies.[22–24]

In this paper we present a fully *ab initio* study of the vibration spectrum, and related properties, of single-walled zigzag BN nanotubes of the (n,0) family. Nanotubes are investigated from $n = 6$ to $n = 60$, that is, from 24 to 240 atoms per cell and from tube radius $R = 2.5$ Å to $R = 24.0$ Å. Vibration frequencies (and their connection with elastic constants), infrared (IR) intensities (and their link with piezoelectricity), oscillator strengths and vibration contributions to the polarizability tensor are illustrated. The convergence, as a function of n, of these properties to the h-BN monolayer limit values is also discussed.

The paper is organized as follows. A detailed description of the methodological and computational setup used

is presented in Section II, in particular as regards the calculation of the vibration frequencies with a full exploitation of symmetry. Results are presented and discussed in Section III, conclusions drawn in Section IV.

II. COMPUTATIONAL DETAILS AND METHOD

All calculations to be reported in the next section have been performed with the CRYSTAL program for quantum chemistry of solid state.[20,21] A split valence plus polarization basis set of Gaussian-type-orbitals (namely a 6-31G* basis set[25,26] with 14 atomic orbitals per atom and 2640 functions per cell in the largest tube) is used in conjunction with the hybrid B3LYP functional of the density functional theory (DFT).[27] The exponents of the most diffuse *sp* shell of each atom have been re-optimized. In CRYSTAL, the truncation of infinite lattice sums is controlled by five thresholds, which are here set to 8,8,8,8,16. The DFT exchange-correlation contribution is evaluated by numerical integration over the cell volume: radial and angular points of the atomic grid are generated through Gauss-Legendre and Lebedev quadrature schemes, using the most accurate predefined pruned grid available: the accuracy in the integration procedure can be estimated by evaluating the error associated to the integrated electronic charge density in the unit cell versus the total number of electrons per cell: 0.001 % for the largest (60,0) nanotube with 1440 electrons per cell. For any further detail about the grid generation and its influence on the accuracy and cost of the calculations, the reader may be addressed to Refs. 28–30. The convergence threshold on energy for the self-consistent-field (SCF) step of the calculations is set to 10^{-8} hartree for geometry optimizations and to 10^{-11} hartree for frequency calculations.

A. Geometry optimizations

All structures have been optimized by use of analytical energy gradients with respect to both atomic coordinates and unit-cell parameters,[31–33] with a quasi-Newton technique combined with the BFGS algorithm for Hessian updating.[34–37] Convergence has been checked on both gradient components and nuclear displacements; the corresponding tolerances on their root mean square are chosen 10 times more severe than the default values: 0.00003 a.u. and 0.00012 a.u., respectively. In order to save computational time and help the convergence of the largest tubes, the optimized geometry of each nanotube n was used to guess the initial geometry of the nanotube n+1 which follows in the (n,0) series; an automatic rebuild option for nanotubes is implemented in the CRYSTAL program (see the documentation of the `NANORE` keyword in the manual).[20]

B. Vibration frequencies

The calculation of vibration frequencies has been performed within the harmonic approximation to the lattice potential. For a detailed description of the method, we refer to previous works.[38,39] Here, let us simply remind that the vibration frequencies at the Γ point ($\mathbf{k} = \mathbf{0}$, at the center of the first Brillouin zone in reciprocal space), those directly comparable to the outcomes of IR measurements, can be obtained from the diagonalization of the mass-weighted Hessian matrix of the second derivatives of the total energy per cell with respect to atomic displacements u:

$$W^{\Gamma}_{ai,bj} = \frac{H^{\mathbf{0}}_{ai,bj}}{\sqrt{M_a M_b}} \quad \text{with} \quad H^{\mathbf{0}}_{ai,bj} = \left(\frac{\partial^2 E}{\partial u^{\mathbf{0}}_{ai} \partial u^{\mathbf{0}}_{bj}} \right) , \quad (1)$$

where atoms a and b (with atomic masses M_a and M_b) in the reference cell are displaced along the i-th and j-th Cartesian directions.

The first derivatives of the total energy per cell ($v_{ai} = \partial E / \partial u_{ai}$) with respect to atomic displacements from the equilibrium configuration $\mathcal{R}^{\mathrm{eq}}$ are computed analytically, whereas second derivatives numerically, using a two-point formula:

$$\frac{\partial^2 E}{\partial u_{ai} \partial u_{bj}} \approx \frac{v_{ai}(\mathcal{R}^{\mathrm{eq}}, u_{bj} = +\overline{u}) - v_{ai}(\mathcal{R}^{\mathrm{eq}}, u_{bj} = -\overline{u})}{2\overline{u}} ,$$

where $\overline{u} = 0.003$ Å, a value 10 - 50 times smaller than that used in other solid state programs.[40–42] In order to check the accuracy of the calculated Hessian, the vibration frequencies of the (10,0) nanotube have been recalculated by using a simpler one point formula: $\partial^2 E / (\partial u_{ai} \partial u_{bj}) = v_{ai}(\mathcal{R}^{\mathrm{eq}}, u_{bj} = +\overline{u}) / \overline{u}$. The mean absolute difference between the two sets is as small as 0.32 cm^{-1} and the maximum difference is only 1.5 cm^{-1}.

The calculation of the vibration frequencies of nanotubes is, in general, a resource demanding problem. The present numerical second derivative scheme would require, in principle, a total number of SCF plus gradients (+G) calculations $N_{SCF+G} = 6\ N_{\mathrm{at}} + 1 = 24n + 1$ for the general (n,0) tube, where N_{at} is the number of atoms per cell and +1 refers to the equilibrium configuration $\mathcal{R}^{\mathrm{eq}}$; this would mean $N_{SCF+G} = 145$ for the (6,0) tube and $N_{SCF+G} = 1441$ for the (60,0) one. If the rich symmetry of this class of materials is fully exploited then N_{SCF+G} reduces to 9 for any tube, irrespective of its size. Out of these 9 SCF+G calculations, 1 exploits the full symmetry ($4n$ operators), 4 exploit 2 operators and other 4 have no left symmetry to be exploited.

C. Born effective tensors

Atomic Born effective tensors $\mathbf{Z}^*_a$ can be computed with the CRYSTAL program by means of a Berry-phase approach.[43,44] Vibrational contributions to the static polarizability α^0, IR intensities and long-range electrostatic

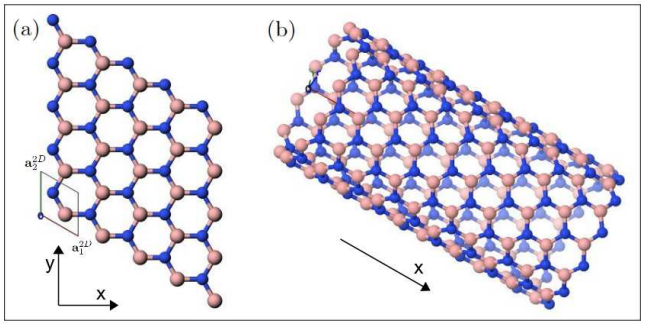

FIG. 1: (color online) Graphical representation of the structure of (a) the h-BN monolayer and (b) a (12,0) BN nanotube. These pictures have been prepared using the J-ICE online interface to Jmol.[50]

force constants can be computed from them. The static polarizability tensor is computed as the sum of the electronic polarizability $\alpha^{\rm el}$ and the vibration contribution $\alpha^{\rm vib}$:

$$\alpha^0_{i,j} = \alpha^{\rm el}_{i,j} + \alpha^{\rm vib}_{i,j} \quad \text{with} \quad \alpha^{\rm vib}_{i,j} = \sum_p \frac{\overline{Z}_{p,i}\overline{Z}_{p,j}}{\nu_p^2} \,. \qquad (2)$$

In the above expression, p labels vibration modes with frequency ν_p, $\overline{\mathbf{Z}}_p$ is the mass-weighted mode effective Born vector[45] and $\alpha^{\rm el}$ can be computed via a coupled-perturbed Hartree-Fock/Konh-Sham (CPHF/KS) scheme.[46–49] The individual contribution $\alpha_{p,i,j} = \overline{Z}_{p,i}\overline{Z}_{p,j}/\nu_p^2$ in equation (2) corresponds to the i,j element of the *oscillator strength* (OS) tensor of mode p. In the present case, all the above mentioned tensors are diagonal by symmetry. The intensity $\mathcal{I}_p$ of IR absorbance for a given mode p is defined as:

$$\mathcal{I}_p = \overline{\mathbf{Z}}_p \cdot \overline{\mathbf{Z}}_p \,. \qquad (3)$$

D. Structural details

The h-BN monolayer conventionally lies in the xy plane, z being the non-periodic direction; it has 2 atoms (*i.e.* 1 BN unit) per cell and then 6 modes at the Γ point (all of them are IR active): three are translations with zero frequency while the other three have vibration frequencies at 836 cm^{-1} (non degenerate) and 1371 cm^{-1} (twofold degenerate). The reader may refer to Figure 1 for a graphical representation of h-BN and corresponding nanotubes. The two lattice vectors $\mathbf{a}_1^{2D}$ and $\mathbf{a}_2^{2D}$ in h-BN form an angle of 60° with each other; $\mathbf{a}_2^{2D}$ is oriented along y and $|\mathbf{a}_2^{2D}| = 2.51$ Å. Nanotubes are one-dimensional periodic structures conventionally oriented along the x direction; y and z are non-periodic directions in this case. The lattice parameter $\mathbf{a}_1^{1D}$ is then oriented along x and $|\mathbf{a}_1^{1D}| = \sqrt{3}|\mathbf{a}_2^{2D}| = 4.35$ Å. Normal modes polarized along non-periodic directions are then twofold degenerate and non-degenerate in nanotubes and monolayer, respectively.

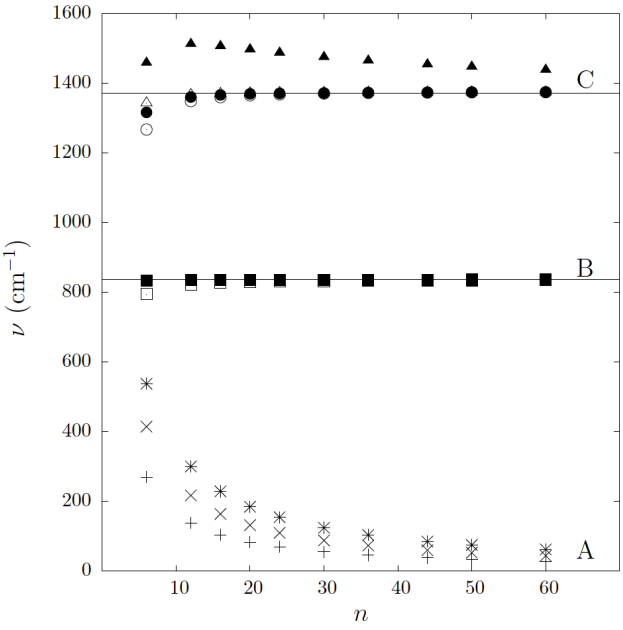

FIG. 2: Convergence of the IR active vibration frequencies of the (n,0) family of BN nanotubes as a function of n to the h-BN monolayer limit (horizontal lines). The frequencies of the band A tend regularly to zero when n increases (see Figure 4).

III. RESULTS AND DISCUSSION

In the (n,0) family of BN nanotubes, there are three sets of IR active modes that we label with letters A, B and C, in the order of increasing frequencies. These sets contains 5, 3 and 6 modes each, respectively; the corresponding frequencies are reported in Table I for all the considered nanotubes. In that table, all non-degenerate modes belong to the totally-symmetric irrep of the group while all twofold degenerate modes, marked with an asterisk, belong to the same bi-dimensional irrep. Figure 2 shows the convergence of the IR active vibration frequencies of the (n,0) family of BN nanotubes as a function of n to the h-BN monolayer limit of 0 cm^{-1} for A, 836 cm^{-1} for B and 1371 cm^{-1} for C. In the following of this section we will discuss these three sets of modes independently. Graphical animations of all these modes can be viewed online.[51]

A. The A set of smooth modes

The A set contains 3 frequencies; the first and third ones, A1* and A3*, are twofold degenerate and the corresponding modes are then polarized in a direction orthogonal to the tube. In A1*, B and N atoms are both displaced along $+x$ at the top of the ring and along $-x$ at the bottom. The variation of the cell (ring) dipole moment is null along x: the xx (parallel, $\|$) component of

the oscillator strength is then $\alpha^{\parallel}_{A1^*} = 0$. Nonetheless, due to the geometry deformation on the equatorial regions of the tube, opposite displacements of B and N atoms of the same unit appear in the yz plane thus making this mode slightly IR active; this leads to non-zero $yy \equiv zz$ (transverse, $\perp$) components of the oscillator strength, see Figure 3 for the dependence on n of this quantity. In the limit $n \to \infty$, this contribution of 0.207 a.u. to the static polarizability tensor is non-vanishing thus corresponding to a piezoelectric effect on the h-BN monolayer, as discussed below.

	A			B		C			
n	1^*	2	3^*	4^*	5	6	7^*	8	9^*
6	269.32	414.41	537.33	794.75	832.58	1266.68	1315.97	1342.44	1458.33
12	137.85	216.88	300.15	822.61	834.58	1348.35	1360.00	1366.52	1512.06
16	103.67	163.81	228.86	826.82	834.86	1359.61	1366.10	1369.77	1505.91
20	83.03	131.50	184.50	829.19	835.20	1364.94	1369.19	1371.54	1496.52
24	69.23	109.73	154.45	830.67	835.43	1367.70	1370.73	1372.35	1487.12
30	55.39	87.88	124.01	832.08	835.73	1370.07	1371.46	1372.50	1474.53
36	46.18	73.29	103.50	832.86	835.78	1371.70	1372.76	1373.47	1464.53
44	37.77	59.94	84.82	833.69	835.96	1372.77	1373.31	1373.76	1453.60
50	33.23	52.69	74.78	834.20	836.17	1373.53	1373.73	1374.04	1446.99
60	27.69	44.00	62.31	834.67	836.24	1373.91	1373.94	1374.13	1438.03
h-BN	0			836		1371			

TABLE I: Vibration frequencies (in cm^{-1}) of the three sets (A, B and C) of IR active modes for h-BN (last row) and BN nanotubes of the (n,0) family as a function of n. The symbol $*$ labels twofold degenerate modes.

The second mode, A2, corresponds to the ring breathing (see animation)[51] and is IR inactive in the yz plane (*i.e.* $\alpha^{\perp}_{A2} = 0$). Opposite displacements of B and N atoms in the x direction make this mode IR active along the periodic direction. In Figure 3 $\alpha^{\parallel}_{A2}$ decreases along the (n,0) series as a function of n, reaching a plateau of 0.195 $\pm$ 0.003 a.u. per BN unit in the $n \to \infty$ limit (value obtained from the fit illustrated in Figure 3). This stretching mode is then creating a non-vanishing polarizability xx component related to the piezoelectricity of the h-BN monolayer (*vide infra*).

The third mode, A3* corresponds to the rigid clockwise rotation in the yz plane of half the ring and anti-clockwise of the other half. The B-N bonds affected by this strain are those at the two borders of these two halves of the ring. Along the x periodic direction, the dipole moment generated by the B-N contraction at one border is annihilated by that generated by the B-N dilation at the other border so that $\alpha^{\parallel}_{A3^*} = 0$. As shown in Figure 3, this mode gives a vanishing contribution to the static polarizability as n increases ($\alpha^{\perp}_{A3^*} = 0.022$ a.u. per BN for $n = 12$, 0.009 a.u. for $n = 30$ and 0.004 a.u. for $n = 60$). This mode does not contribute to the piezoelectricity of the h-BN monolayer. In summary, the A1* and A2 modes only are contributing to the polarizability for large n.

1. *Connection with elastic tensor*

In Figure 4 we report the three vibration frequencies of the the A set of (n,0) nanotubes as a function of $1/n$. A linear behavior is observed which is confirmed by the results of a linear fitting (lines shown in the figure). From inspection of the figure, it clearly emerges that the vibration frequencies of these modes vanish in the limit $n \to \infty$. The slopes of the three lines, reported in the figure, are 1675, 2688 and 3862 cm^{-1} for A1*, A2 and A3*, respectively. As discussed in what follows, the values of these slopes can be related to the components of the symmetryc elastic tensor $\mathbb{C}$ of the h-BN monolayer. The elements of the elastic tensor are usually defined, for 3D systems, as:[52]

$$C_{vu} = \frac{1}{V} \left. \frac{\partial^2 E}{\partial \epsilon_v \partial \epsilon_u} \right|_0 , \qquad (4)$$

where ϵ is the rank 2 symmetric tensor of pure strain and Voigt's notation has been used according to which $v, u = 1, \ldots, 6$ ($1 = xx$, $2 = yy$, $3 = zz$, $4 = yz$, $5 = xz$,

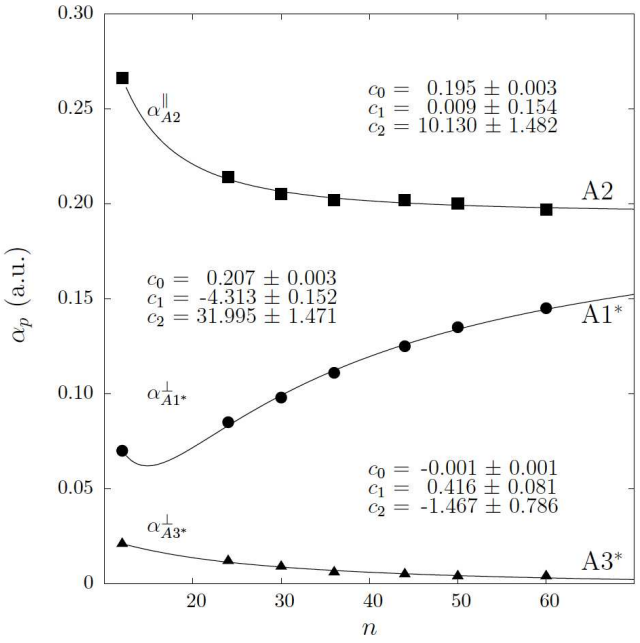

FIG. 3: Vibrational contribution α_p to the polarizability tensor (oscillator strength) of the three modes of the A set of (n,0) BN nanotubes, as a function of n (values in a.u. per BN unit). For A1 we report the $yy \equiv zz$ component, for A2 the xx and for A3 the $yy \equiv zz$ ones. Data-points have been fitted to the function: $\alpha_p = c_0 + c_1/n + c_2/n^2$; the coefficients obtained using the 6 largest tubes are reported in the figure.

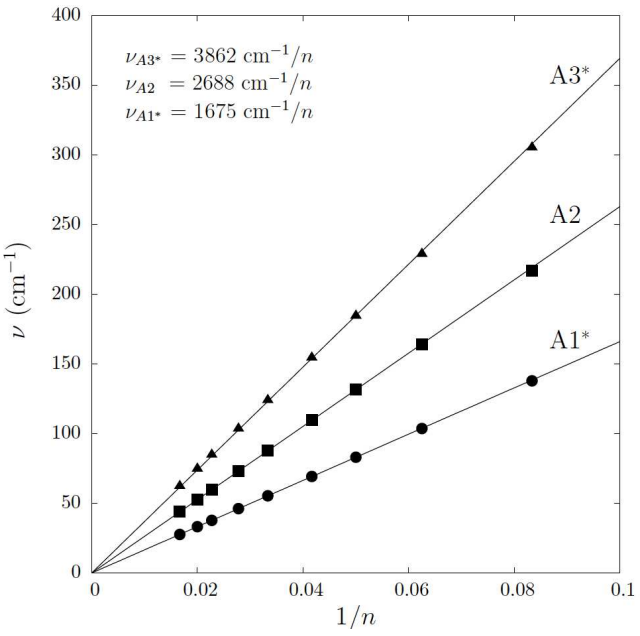

FIG. 4: Vibration frequencies of the A set of IR active modes as a function of $1/n$ in the (n,0) series of nanotubes. The results of a linear fitting are shown as well.

$6 = xy$). For a 2D system, the volume V is not defined and is omitted (note that a surface unit could be used instead) and all the elements involving the non-periodic direction z are null by definition. Due to the hexagonal symmetry of the h-BN monolayer, its elastic tensor $\mathbb{C}$ thus exhibits the following structure:

$$\mathbb{C} = \begin{vmatrix} C_{11} & C_{12} & 0 \\ C_{12} & C_{11} & 0 \\ 0 & 0 & \frac{1}{2}(C_{11} - C_{12}) \end{vmatrix} . \qquad (5)$$

The elements of this tensors are known as elastic constants; they have been computed for the h-BN monolayer. Let us give explicitly the values of two of them to be used below: $C_{22} = C_{11} = 3.954$ hartree and $C_{66} = 1/2(C_{11} - C_{12}) = 1.630$ hartree.

Now we start looking for the connection between the vibration frequencies reported in Figure 4 and the elastic constants of h-BN. We consider first the A2 mode of the ring breathing; for n large enough, the frequencies depend only on the elastic constant of the monolayer and on the deformation induced by the vibrational mode. The energy of the mode $E^{\rm vib}$ of a (n,0) tube should then be equal to the energy required to induce an equivalent deformation of the $2n$ BN units in the monolayer $E^{\rm elast}$:

$$E^{\rm vib} = E^{\rm elast} \quad \rightarrow \quad \frac{1}{2}\nu_{A2}^2 Q_{A2}^2 = nC_{22}\epsilon_2^2 \, , \qquad (6)$$

where Q_{A2} is the harmonic normal coordinate of the mode and $\epsilon_2 \equiv \epsilon_{yy} = \delta|\mathbf{a}_2^{2D}|/|\mathbf{a}_2^{2D}|$ is the parallel component of the strain tensor in the monolayer. In the $n \rightarrow \infty$ limit, when the ring width $\mathbf{a}_1^{1D}$ becomes irrelevant compared to the tube radius R_n we can write:

$$Q_{A2} = \sqrt{2n(M_B + M_N)}\delta R_n \, , \qquad (7)$$

where M_B and M_N are the atomic masses of B and N atoms. The corresponding distortion in the monolayer is a dilatation of the cell. As $2\pi R_n = n|\mathbf{a}_2^{2D}|$ and $\delta R_n/R_n = \delta|\mathbf{a}_2^{2D}|/|\mathbf{a}_2^{2D}| = \epsilon_2$ and substituting equation (7) into equation (6), we obtain:

$$\nu_{A2} = \sqrt{\frac{C_{22}}{(M_B + M_N)R_n^2}} = \sqrt{\frac{C_{22}}{(M_B + M_N)}} \frac{2\pi}{|\mathbf{a}_2^{2D}|} \frac{1}{n} \, .$$

From the above expression, by using the calculated value of C_{22} and $|\mathbf{a}_2^{2D}| = 2.51$ Å, we get $\nu_{A_2} = 2725$ cm^{-1} $/n$, to be compared to the value of 2688 cm^{-1} obtained from the linear fitting in Figure 4. The same procedure can be followed for the A1* twofold degenerate mode (see Appendix A) that is related to the ϵ_6 component of the strain tensor and to the C_{66} elastic constant of the monolayer. At the end, one gets $\nu_{A1^*} = 1749$ cm^{-1} $/n$ somehow close to the value 1675 cm^{-1} obtained from the fit in Figure 4. The strain induced by the twofold degenerate A3* mode is similar to that of the A2 mode so that the corresponding elastic constant is C_{22} again (see animation);[51] the only difference is that the reduced mass is half the mass of the total ring so that, at the end, one finds $\nu_{A3^*} = \sqrt{2}\nu_{A2} = 3854$ cm^{-1} $/n$, which is

comparable to the value 3862 cm^{-1} obtained from the fitting of Figure 4. Bearing in mind that this comparison passes through the computation of very different quantities (vibration frequencies of the nanotubes and elastic constants of the monolayer), the agreement can be considered rather impressive.

2. *Connection with piezoelectric tensor*

As shown in Figure 3, the A band provides a non-vanishing contribution to the polarizability tensor in the $n \to \infty$ limit. In particular, the A1* mode gives a limit value of 0.207 a.u. per BN unit to the $yy \equiv zz$ transverse components while the A2 mode 0.195 a.u. per BN unit to the xx parallel component. These non-vanishing contributions can be related to the piezoelectricity of the h-BN monolayer. The piezoelectric (rank 3) tensor **e** elements can be defined as (in Voigt's notation):[53,54]

$$e_{iv} = \left.\frac{\partial P_i}{\partial \epsilon_v}\right|_0 , \qquad (8)$$

where P is the polarization, $i = 1,\ldots,3$ while $v = 1,\ldots,6$ is one of the strain components and the derivative is calculated at zero strain. As discussed before for the elastic tensor, for 2D systems all the components involving the non-periodic direction z vanish. The piezoelectric tensor for the h-BN monolayer has been computed; we report the values of two components (equal by virtue of symmetry) to be used later: $e_{12} \equiv e_{26} = 2.28$ a.u..

The oscillator strengths, OS, (directly related to the IR intensities, see equation 3) of the A modes have been fitted to the function: $\alpha_p(n) = c_0 + c_1/n + c_2/n^2$. From the results of this fit, reported in Figure 3, it clearly emerges the $1/n^2$ character of the OS and, as a consequence, of IR intensities of both A1* and A2 while the corresponding vibration frequencies have a $1/n$ character (see Figure 4).

Let us consider the simple symmetric A2 mode (ring breath). In this case the dipole moment of the tube ($\delta\mu_x$) per unit length induced along the periodic x direction can be related to the dipole moment of a h-BN unit cell ($\delta\mu_x^{2D}$) induced by the deformation ϵ_2 in the slab. Since all the microscopic dipole moments generated by the symmetric A2 mode on the ring are equal to each other along x, $\delta\mu_x$ is equal to n times the dipole moment of each hexagon $(BN)_3$ constituting the ring of the tube. Since there are 2 BN units per hexagon, the intensity of the mode per BN unit can be written as follows:

$$\frac{1}{2n}\left(\frac{\delta\mu_x}{\delta Q_{A2}}\right)^2 = \frac{1}{3n}\left(\frac{n\delta\mu_x^{2D}}{\sqrt{2n(M_B+M_N)}n\delta|\mathbf{a}_2^{2D}|/2\pi}\right)^2 = \frac{1}{6}\frac{4\pi^2}{(M_B+M_N)(|\mathbf{a}_2^{2D}|)^2}\left(\frac{\delta\mu_x^{2D}}{\epsilon_2}\right)^2\frac{1}{n^2} .$$

We can notice that the intensity of the A2 mode per BN unit is proportional to $1/n^2$. The vibrational contribution of A2 to the parallel polarizability of the tube is then:

$$\alpha_{A2}^{\parallel} = \frac{1}{\nu_{A2}^2}\left(\frac{\delta\mu_x}{\delta Q_{A_2}}\right)^2 = \frac{1}{6}\frac{e_{12}^2}{C_{22}} , \qquad (9)$$

where e_{12} is the "microscopic" piezoelectric component of the h-BN monolayer. From the computed values of e_{12} and C_{22} for the monolayer, we get $\alpha_{A2}^{\parallel} = 0.22$ a.u., to be compared with the value obtained for this parallel vibrational component of the polarizability of the nanotubes in the $n \to \infty$ limit from the fit of Figure 3: 0.20 a.u.

For the A1* mode, its contribution to the transverse polarizability can be obtained as $\alpha_{A1^*}^{\perp} = e_{26}^2/(16C_{66}) = 0.20$ a.u. to be compared with the direct calculation of the polarizability component of the nanotubes in the $n \to \infty$ limit: 0.21 a.u. For a detailed discussion of this case, see Appendix B.

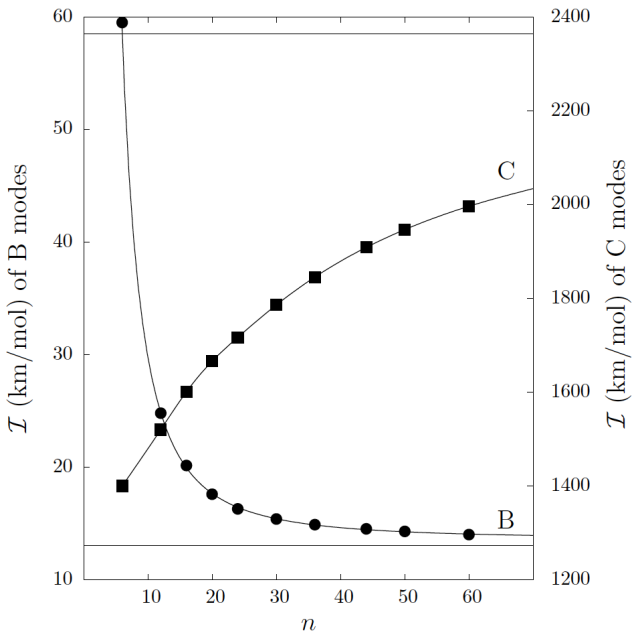

FIG. 5: Convergence of the IR intensity of modes B (full circles) and C (full squares) of (n,0) BN nanotubes as a function of n. The corresponding values for the h-BN monolayer are reported as horizontal lines. The last 6 points of the two sets of data have been fitted to the function $\mathcal{I}_p = c_0 + c_1/n + c_2/n^2$; The coefficients of the fitting are $c_0 = 13.20$, $c_1 = 44$ and $c_2 = 1137$ for B and $c_0 = 2303$, $c_1 = -21296$ and $c_2 = 173474$ for C.

B. The B and C sets of modes

The B and C sets of modes correspond to opposite displacements of B and N atoms of the same unit and are directly related to the vibration modes of the h-BN monolayer in the $n \to \infty$ limit. As marked in Table I, the lowest frequency of the B set and the first and third ones of the C set are twofold degenerate. As shown in Figure

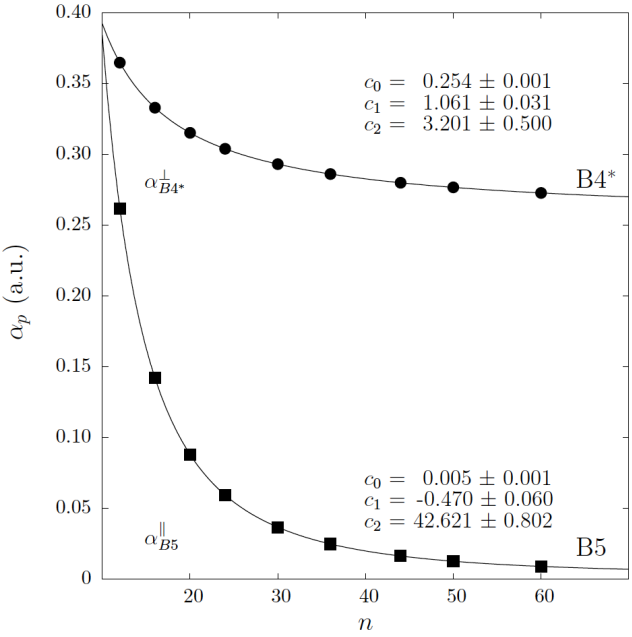

FIG. 6: Vibrational contributions to the polarizability tensor (oscillator strengths α_p) of the two modes of the B set of (n,0) BN nanotubes, as a function of n (values in a.u. per BN unit). Data-points have been fitted to the function: $\alpha_p = c_0 + c_1/n + c_2/n^2$; the coefficients obtained using the 6 largest tubes are reported in the figure.

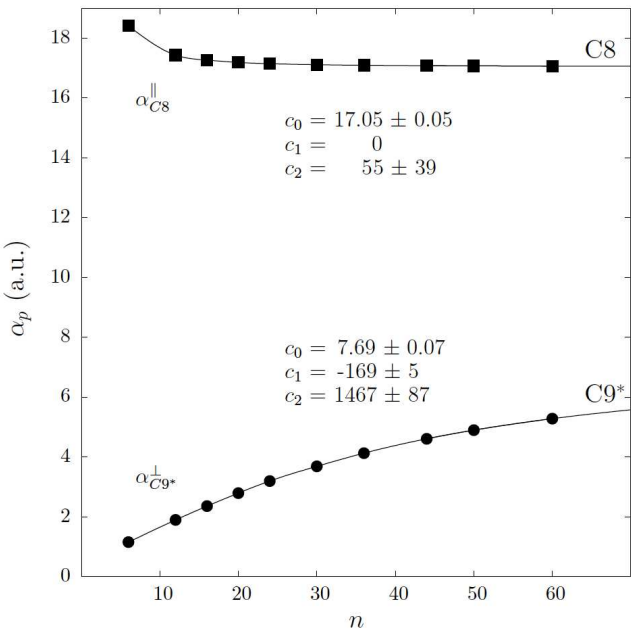

FIG. 7: As in Figure 6 for the C set of modes.

2, one of the two frequencies in the B band is already quite close to the h-BN limit for $n = 6$ while the second one starts from 794 cm^{-1} when $n = 6$ and ends up at 834.7 cm^{-1} at $n = 60$, at just 1 cm^{-1} from the h-BN value. The C band is about 200 cm^{-1} wide at $n = 6$; at $n = 60$ three out of four frequencies are very close to the h-BN value of 1371 cm^{-1}, whereas the last one remains about 70 cm^{-1} higher and decreases very slowly: in this case, the extrapolation to $n = \infty$ still differs by about 10 cm^{-1} from the monolayer limit.

In Figure 5 we report the behavior of the IR intensity $\mathcal{I}_p$ of B and C modes as a function of n. The last 6 points in the series, corresponding to the largest tubes, have been fitted to the function $\mathcal{I}_p = c_0 + c_1/n + c_2/n^2$. As regards B, apart from the $n = 6$ case that shows an anomalous high intensity ($\approx$ 60 km/mol), the intensity decreases quite regularly along the series with a strong $1/n^2$ character. The c_0 coefficient, that gives the value of the intensity in the $n \to \infty$ limit, is 13.20 km/mol, to be compared with the h-BN value of 13.06 km/mol (horizontal line at the bottom of Figure 5). The situation is different for the intensities of the C modes. In this case the $n = 6$ case is in line with the larger tubes; the IR intensity increases very slowly in this case; even at the largest tube, $n = 60$, the intensity (1998 km/mol) is still very far from the h-BN limit (2371 km/mol). From the fit, however, an asymptotic value of 2303 km/mol is obtained which is only 3 % smaller than the h-BN value.

Let us analyze into detail the B and C modes. The B4* mode is twofold degenerate and represents opposite displacements of B and N atoms of the same unit perpendicularly to the ring, in the yz plane. An oscillating dipole moment is created so that this mode is IR active; given the nature of this mode, the polarizability component $\alpha^{\perp}_{B4^*}$ of the tube tends (in the $n \to \infty$ limit) to half the vibrational perpendicular component $\alpha^{2D}_{zz} = 0.506$ a.u. of the polarizability of the slab (see Table IV of Ref. 22). In Figure 6, we report such quantity as a function of n along the (n,0) nanotube series. The last 6 points, corresponding to the 6 largest tubes here considered, have been fitted to the function: $\alpha_p = c_0 + c_1/n + c_2/n^2$; the coefficients obtained are reported in the figure. From the fitting we obtain $\alpha^{\perp}_{B4^*} = 0.254 \pm 0.001$ a.u. to be compared with $\alpha^{2D}_{zz}/2 = 0.253$ a.u.

The B5 mode is somehow similar to the A2 ring breath except that B and N atoms of the same BN unit are displacing in opposite directions: when the sub-ring of B atoms is contracted, the N atoms sub-ring is dilated and vice versa. As a consequence of its symmetry, the mode is IR inactive in the yz plane since the projection of the dipole moment in the yz plane is null ($\alpha^{\perp}_{B5} = 0 \ \forall n$) but a strain along x makes the mode slightly IR active in the periodic direction, at least in the limit of small n's. Indeed, it is seen from Figure 6 that the component $\alpha^{\parallel}_{B5}$ of the polarizability regularly decreases to zero as a function of n. This mode becomes IR inactive in the $n \to \infty$ limit.

The first two modes, C6 and C7*, of the C set are IR inactive ($\alpha^{\parallel} = \alpha^{\perp} = 0 \ \forall n$) while the other two, C8 and C9*, are IR active. The C8 mode represents opposite displacements of B and N atoms of the same unit in the x-direction all around the ring. In this case, the non-

zero polarizability component is $\alpha^{\parallel}_{C8}$ which tends (in the $n \to \infty$ limit) to the parallel component of the monolayer α^{2D}_{xx}. In Figure 7, we report such quantity as a function of n. As done before for the B set, the last 6 points have been fitted to the function: $\alpha_p = c_0 + c_1/n + c_2/n^2$ and the corresponding coefficients reported in the figure. From the fitting we obtain $\alpha^{\parallel}_{C8} = 17.05 \pm 0.05$ a.u. to be compared with $\alpha^{2D}_{xx} = 17.01$ a.u., see Table IV of Ref. 22.

C9* is similar to B4* but where the opposite displacements of B and N atoms of the same unit are along the ring. In this case, the transverse component $\alpha^{\perp}_{C9^*}$ tend slowly to $\alpha^{2D}_{xx}/2$ as a function of n. From the fit reported in Figure 7, a limit value of 7.69 ± 0.07 a.u. is obtained to be compared with $\alpha^{2D}_{xx}/2 = 8.50$ a.u..

IV. CONCLUSIONS

In this paper we have investigated the vibration spectrum of single-walled zigzag BN nanotubes of the $(n,0)$ family, where n is an integer defining the tube size, by means of *ab initio* quantum chemical simulations. We have considered tubes up to $n = 60$ with 240 atoms and 2640 basis functions per cell. A program, CRYSTAL, has been used that fully exploits the rich symmetry of this class of one-dimensional periodic systems. A variety of properties related to the vibrational spectrum have been computed, from vibration frequencies and infrared intensities to oscillator strengths and vibration contributions to the polarizability tensor. The trend towards the hexagonal monolayer (h-BN) in the limit of large tube radius has also been explored.

In the vibration spectrum, there are three sets of IR active phonon bands. The first one, A, lies in the 0 - 600 cm^{-1} range and the corresponding frequencies go regularly to zero when n increases; the connection between these normal modes and both the elastic and piezoelectric tensors of the h-BN monolayer has been illustrated. The second, B, (600 - 800 cm^{-1}) and third, C, (1300 - 1600 cm^{-1}) sets tend regularly to the optical modes of the h-BN layer. The vibrational contribution of these modes to the polarizability tensor of the tubes and their connection to the polarizability of the h-BN monolayer have been presented.

From the complete solution of the lattice dynamical problem (*i.e.* from complete phonon dispersion), other quantities could be computed such as thermodynamic properties, phonon bands, inelastic neutron scattering spectra, atomic anisotropic displacement parameters and Debye-Waller factors. Such an investigation is currently in progress for this class of materials.

Acknowledgments

The authors acknowledge the CINECA Award N. HP10AC4ZGA-2010 for the availability of high performance computing resources and support. Manipulation and visualization of structures have been performed with the MOLDRAW program (http://www.moldraw.unito.it) and the Jmol 3D engine (http://jmol.sourceforge.net/).

Appendix A: Link between vibration frequency and elastic constants for the A1* modes

In Section III A 1 we have discussed the connection between the vibration frequencies of the A set of modes of the nanotubes, as n increases, and the elastic constants of the h-BN monolayer. To do so, we should equal the energy of the mode to that required for inducing an equivalent deformation in the monolayer:

$$E^{\rm vib} = E^{\rm elast} \ . \tag{A1}$$

Let us consider here in detail the case of the A1* modes. Given the nature of these modes, for large values of n, the corresponding distortion in h-BN is not of the size of the unit cell but of the lattice angles. The elastic constant involved is thus C_{66} and the corresponding component of the strain tensor ϵ_6. The general atomic displacement l along the periodic direction x is not uniform along the circumference of the tube as was in the case of the A2 mode; since the ring is inclined of an angle ϕ with respect to x, the displacement l is proportional to the distance d of the atom from the rotation axis of the mode (y or z in the two degenerate modes):

$$l = d\sin\phi = R_n \sin\theta \sin\phi \ , \tag{A2}$$

where θ is an angle that spans the circumference of the tube: $\theta = 0$ corresponds to the mode axis.

The vibration energy of the A1* mode $E^{\rm vib} = 1/2\nu^2_{A1^*}Q^2_{A1^*}$ depends on the corresponding normal coordinate Q_{A1^*}; in order to obtain its expression, we can make the sensible approximation of considering the ring (tube cell) as an uniform ring of mass m; in this case we can write:

$$\begin{aligned} Q^2_{A1^*} = \int l^2 {\rm d}m &= 2\int_0^{\pi} (R_n \sin\theta \sin\phi)^2 \rho R_n {\rm d}\theta \\ &= 2R_n^3 \rho \frac{\pi}{2} \sin^2\phi \\ &= n(M_N + M_B)\sin^2\phi \ , \end{aligned} \tag{A3}$$

where $\rho = 2n(M_N + M_B)/2\pi R_n$ is the linear mass density. The mode energy is then:

$$E^{\rm vib} = \frac{1}{2}\nu^2_{A1^*} n(M_N + M_B)\sin^2\phi \ . \tag{A4}$$

The elastic energy is $E^{\rm elast} = nC_{66}\epsilon_6^2$; the strain component ϵ_6 is the derivative of the atomic displacement:

$$\epsilon_6 = \frac{{\rm d}l}{{\rm d}\mathbf{r}} = \frac{R_n \sin\phi}{R_n} \frac{{\rm d}\,\sin\theta}{{\rm d}\theta} = \sin\phi\cos\theta \ . \tag{A5}$$

The elastic energy can then be written as:

$$E^{\rm elast} = \frac{n}{\pi}\int_{-\pi/2}^{+\pi/2} C_{66}\sin^2\phi\cos^2\theta \mathrm{d}\theta = \frac{n}{2}C_{66}\sin^2\phi\ . \quad \text{(A6)}$$

Using $2\pi R_n = n|\mathbf{a}_2^{2D}|$, considering that $E^{\rm vib} = E^{\rm elast}$ and exploiting equations (A4) and (A6) we obtain:

$$\nu_{A1^*} = \sqrt{\frac{C_{66}}{(M_B+M_N)}}\frac{2\pi}{|\mathbf{a}_2^{2D}|}\frac{1}{n}\ , \quad \text{(A7)}$$

that provides the desired connection between the vibration frequency of the tube and the elastic constant of the monolayer for the $A1^*$ modes.

Appendix B: Link between vibration frequency and piezoelectricity for the A1* modes

[... Michel? ...]

[1] S. Ijima, Nature **354**, 96 (1991).
[2] M. U. Kahaly and U. V. Waghmare, J. Nanoscience and Nanotechnology **7**, 1787 (2007).
[3] A. Rubio, J. Corkill, and M. Cohen, Phys. Rev. B **49**, 5081 (1994).
[4] X. Blase, A. Rubio, S. Louie, and M. Cohen, Europhys. Lett. **28**, 335 (1994).
[5] N. Chopra, R. Luyken, V. Crespi, M. Cohen, S. Louie, , and A. Zettl, Science **269**, 966 (1995).
[6] C. Sun, H. Yu, L. Xu, Q. Ma, and Y. Qian, Journal of Nanomaterials (2010).
[7] D. Golberg, Y. Bando, C. C. Tang, and C. Y. Zhi, Advanced Materials **19**, 2413 (2007).
[8] C. Zhi, Y. Bando, C. Tang, and D. Golberg, Materials Science and Engineering: R: Reports **70**, 92 (2010).
[9] S. Hao, G. Zhou, W. Duan, J. Wu, and B. L. Gu, J. Am. Chem. Soc. **128**, 8453 (2006).
[10] G. Y. Guo, S. Ishibashi, T. Tamura, and K. Terakura, Phys. Rev. B **75**, 245403 (2007).
[11] G. Y. Guo and J. C. Lin, Phys. Rev. B **71**, 165402 (2005).
[12] S. Z. Hai-Ping Lan, Lin-Hui Ye and L.-M. Peng, Appl. Phys. Lett. **94**, 183110 (2009).
[13] H. Dai, Acc. Chem. Res. **35**, 1035 (2002).
[14] C. T. White, D. H. Robertson, and J. W. Mintmire, Phys. Rev. B **47**, 5485 (1993).
[15] V. Barone and G. E. Scuseria, J. Chem. Phys. **121**, 10376 (2004).
[16] P. V. Avramov, K. N. Kudin, and G. E. Scuseria, Chem. Phys. Lett. **370**, 597 (2003).
[17] E. N. Brothers, G. E. Scuseria, and K. N. Kudin, J. Phys. Chem. B **110**, 12860 (2006).
[18] Y. Noël, P. D'Arco, R. Demichelis, C. M. Zicovich-Wilson, and R. Dovesi, J. Comput. Chem. **31**, 855 (2010).
[19] C. M. Zicovich-Wilson, Y. Noël, A. M. Ferrari, R. Orlando, M. D. L. Pierre, and R. Dovesi, AIP Conference Proceedings **1456**, 248 (2012).
[20] R. Dovesi, V. R. Saunders, C. Roetti, R. Orlando, C. M. Zicovich-Wilson, F. Pascale, K. Doll, N. M. Harrison, B. Civalleri, I. J. Bush, et al., *CRYSTAL09 User's Manual*, Università di Torino, Torino (2010), http://www.crystal.unito.it.
[21] R. Dovesi, R. Orlando, B. Civalleri, C. Roetti, V. R. Saunders, and C. M. Zicovich-Wilson, Z. Kristallogr. **220**, 571 (2005).
[22] M. Ferrabone, B. Kirtman, R. Orlando, Rérat, and R. Dovesi, Phys. Rev. B **83**, 235421 (2011).
[23] M. Ferrabone, B. Kirtman, V. Lacivita, M. Rérat, R. Orlando, and R. Dovesi, Int. J. Quantum Chem. **112**, 2160 (2012).
[24] R. Orlando, R. Bast, K. Ruud, U. Ekström, M. Ferrabone, B. Kirtman, and R. Dovesi, J. Phys. Chem. A **115**, 12631 (2011).
[25] D. Feller, J. Comp. Chem. **17** (1996).
[26] K. Schuchardt, B. Didier, T. Elsethagen, L. Sun, V. Gurumoorthi, J. Chase, J. Li, and T. Windus, J. Chem. Inf. Model. **47** (2007).
[27] A. D. Becke, J. Chem. Phys. **98**, 5648 (1993).
[28] F. Pascale, C. M. Zicovich-Wilson, R. Orlando, C. Roetti, P. Ugliengo, and R. Dovesi, J. Phys. Chem. B **109**, 6146 (2005).
[29] M. Prencipe, F. Pascale, C. Zicovich-Wilson, V. Saunders, R. Orlando, and R. Dovesi, Phys. Chem. Min. **31**, 559 (2004).
[30] S. Tosoni, F. Pascale, P. Ugliengo, R. Orlando, V. R. Saunders, and R. Dovesi, Mol. Phys. **103**, 2549 (2005).
[31] K. Doll, Comput. Phys. Comm. **137**, 74 (2001).
[32] K. Doll, N. M. Harrison, and V. R. Saunders, Int. J. Quantum Chem. **82**, 1 (2001).
[33] B. Civalleri, P. D'Arco, R. Orlando, V. R. Saunders, and R. Dovesi, Chem. Phys. Lett. **348**, 131 (2001).
[34] C. G. Broyden, J. Inst. Math. Appl. **6**, 76 (1970).
[35] R. Fletcher, Comput. J **13**, 317 (1970).
[36] D. Goldfarb, Math. Comput. **24**, 23 (1970).
[37] D. F. Shanno, Math. Comput. **24**, 647 (1970).
[38] F. Pascale, C. M. Zicovich-Wilson, F. L. Gejo, B. Civalleri, R. Orlando, and R. Dovesi, J. Comp. Chem. **25**, 888 (2004).
[39] C. M. Zicovich-Wilson, F. Pascale, C. Roetti, V. R. Saunders, R. Orlando, and R. Dovesi, J. Comp. Chem. **25**, 1873 (2004).
[40] J. M. Soler, E. Artacho, J. D. Gale, A. García, J. Junquera, P. Ordejón, and D. Sánchez-Portal, J. Phys.-Condens. Mat. **14**, 2745 (2002).
[41] G. Kresse and J. Furthmüller, Comput. Mat. Sci. **6**, 15 (1996).
[42] G. Kresse and J. Furthmüller, Phys. Rev. B **54**, 11169 (1996).
[43] R. Resta, Rev. Mod. Phys. **66**, 809 (1994).
[44] R. D. King-Smith and D. Vanderbilt, Phys. Rev. B **49**, 5828 (1994).
[45] X. Gonze and C. Lee, Phys. Rev. B **55**, 10355 (1997).
[46] M. Ferrero, M. Rérat, R. Orlando, and R. Dovesi, J. Comp. Chem. **29**, 1450 (2008).
[47] M. Ferrero, M. Rérat, B. Kirtman, and R. Dovesi, J. Chem. Phys. **129**, 244110 (2008).
[48] M. Ferrero, M. Rérat, R. Orlando, R. Dovesi, and I. J. Bush, J. Phys.: Conference SeriesIOP Publishing **117**, 012016 (2008).

[49] M. Ferrero, B. Civalleri, M. Rérat, R. Orlando, and R. Dovesi, J. Chem. Phys. **131**, 214704 (2009).
[50] P. Canepa, R. Hanson, P. Ugliengo, and M. Alfredsson, J. Appl. Cryst. **44**, 225 (2011).
[51] http://www.crystal.unito.it/vibs/BN_nanotubes/BN-OPT-NANO-60-ND2/.
[52] W. F. Perger, J. Criswell, B. Civalleri, and R. Dovesi, Comput. Phys. Commun. **180**, 1753 (2009).
[53] Y. Noel, M. Llunell, R. Orlando, P. D'Arco, and R. Dovesi, Phys. Rev. B **66**, 214107 (2002).
[54] M. Catti, Y. Noel, and R. Dovesi, J. Phys. Chem. Solids **64**, 2183 (2003).